INFLUENCE OF UNIFORM ELECTRON CLOUDS ON THE COUPLING IMPEDANCE*

A.M. Al-Khateeb, Yarmouk University, Irbid, Jordan,
R.W. Hasse, O. Boine-Frankenheim, GSI Darmstadt, Darmstadt, Germany

Abstract

The contribution to the longitudinal coupling impedance from an electron cloud in the form of a uniformly distributed non-neutral plasma of electrons is investigated analytically. The beam-pipe is assumed to be of circular cross section with a thick resistive wall. The beam charge distribution is uniform in the transverse direction. The electron contribution to the charge and current densities are obtained from the collective electron response to the beam passage through the pipe. We obtain the radial differential equation governing the field variation in the presence of the electron background and a general closed formula for the longitudinal coupling impedance is derived. The depletion of the coupling impedance with the density of the electron cloud is discussed for the examples of GSI SIS-18 and SIS-100, CERN SPS and PS, and the KEKB LER, and conditions for the minimum excitation frequency as a function of the electron density are derived. Furthermore, the case of over-dense plasmas is also studied.

INTRODUCTION

During the recent years clouds of electrons have been found in circular accelerators with high energy high current ion beams which evidently are created by protons (or ions) hitting the walls in the dipoles or elsewhere. In the walls avalanches of electrons are generated which give rise to clouds of electrons. The ion charges disturb the original beam and give rise to instabilities.

Examples where such instabilities were observed are the KEKB Low Energy Ring (LER) [1], and the CERN Proton Synchrotron (PS) [2] and Super Proton Synchrotron (SPS) [3], and at the Relativistic Heavy Ion Collider (RHIC) [4]. For a review see Zimmermann [5]; the CERN webpage on electron clouds (EC) [6], and for recent simulations see ref. [7, 8]. The instabilities manifest themselves in single bunches due to multiple transitions of a bunch through the EC [5, 7]. In the SPS the single-bunch instability affects the last two thirds of the batch. Also, vertical instabilities have been observed of single bunch nature, its growth rate depending on intensity. The vertical instability seems to be enhanced by the machine impedance around $600\cdots800$ MHz. On the other hand, the wake-field generated by the EC may influence the low density region between heads and tails of the bunches, see e.g. ref. [8]. This, in turn, results in a fast horizontal coupled bunch instability of low order that may be cured by a feedback system. In the SPS as well as in the LER electron cloud densities of $n_{\rm ec} = 10^{11}\cdots10^{12}$ m^{-3} have been detected. The EC, however, not only generates a wake-field but it also modifies the impedance coming from coupling of the beam to the resistive wall.

In the present paper we study this effect by simply assuming a homogeneous EC of density $n_{\rm ec}$ spreading all over the interior of the aperture which holds the charged particle beam. Here the EC acts like shielding the beam which, in turn, gives rise to a depletion of the coupling impedances. This depletion then is calculated as a function of the electron cloud plasma frequency $\omega_{\rm ec}$, namely,

$$\omega_{\rm ec} = \sqrt{\frac{n_{\rm ec}e^2}{m_{\rm e}\epsilon_0}}\ , \qquad (1)$$

where $m_{\rm e}$ is the electron mass, e is the elementary charge, and ϵ_0 is the permittivity of free space. For the electron densities given above the electron plasma frequencies are of the order of $f_{\rm ec} = \omega_{\rm ec}/2\pi$ = $1\cdots10$ MHz. It turns out that this is effect is governed by the ratio $\omega_{\rm ec}/\omega$ with ω being the excitation frequency. The results are applied to the circular machines CERN SPS and PS, KEKB LER and GSI SIS-18 and the proposed SIS-100. As a stability criterion for low energy machines $\omega_{\rm ec}/\omega \lesssim 0.5$ must be fulfilled but for the high energy machines $\omega_{\rm ec}/\omega \ll 1$ is necessary. Qualitatively, hence, we see that for low frequencies the appearance of instabilities is favoured by electron clouds. In the next sections we will study this effect quantitatively.

ELECTRON CLOUD CONTRIBUTION TO THE SOURCES

Consider the motion of a rotationally symmetric lamina of particles of radius a and total charge Q in a smooth cylindrical pipe of radius b and circumference L. The beam moves in this nonneutral plasma with a constant longitudinal velocity $\vec{v}_b = \beta c\hat{z}$ along the z axis through a uniform electron background of density $n_{\rm ec}$ electrons per unit volume which fills the whole pipe up to radius b, each of mass $m_{\rm e}$, and of charge $-e$. The total (effective) current $\vec{J}$ and charge $\rho(\vec{r},t)$ densities are defined as follows,

$$\begin{aligned}\vec{J}(\vec{r},t) &= \vec{j}_0 + \vec{j}_{\rm e}\ , \qquad (2)\\ \rho &= \rho_0 + \rho_{\rm e}\ .\end{aligned}$$

In following along the lines Mulsers oscillator model [9], the current $\vec{j}_0$ and charge ρ_0 densities in eq. (2) are those associated with the streaming motion of the beam particles, whereas $\vec{j}_{\rm e}$ and $\rho_{\rm e}$ are the collective current and charge

[1]Proc. Beam07 CARE-HHH-APD Workshop, CERN, 1-5 Oct. 2007

densities due to the coupling between the background electrons and the excited electric fields in the cylindrical pipe. For cold, collisionless, unmagnetized electron background, the electron equation of motion in the effective electromagnetic field is,

$$\frac{d\vec{j}_{\rm e}}{dt} = \frac{e^2 n_{0ec}}{m_{\rm e}}\,\vec{E} - \frac{e}{m_{\rm e}}\,\vec{j}_{\rm e}\times\vec{B}\,. \tag{3}$$

Fourier transforming in time, for the transverse magnetic (TM) modes of lower order $\ell = 0$ corresponding to axially symmetric transverse beam charge distribution, and by ignoring the $\vec{E}\times\vec{B}$ drift of the electron background, we obtain the following simple expression for the effective induced EC current density, namely,

$$\vec{j}_{\rm e} = \frac{i\omega e^2 n_{0ec}}{m_{\rm e}\omega^2}\,\vec{E}\,, \tag{4}$$

$$\frac{\partial^2\rho_{\rm e}}{\partial t^2} + \vec{\nabla}\cdot\frac{d\vec{j}_{\rm e}(\vec{r},t)}{dt} = \frac{\partial^2\rho_{\rm e}}{\partial t^2} + \frac{e^2 n_{0ec}}{m}\,\vec{\nabla}\cdot\vec{E}(\vec{r},t) = 0\,.$$

Upon using Faraday's and Ampere's laws, the wave equations satisfied by the magnetic induction $\vec{B}$ and the electric field $\vec{E}$ in nonconducting media with $\epsilon = \epsilon_0$ and $\mu = \mu_0$ are,

$$\nabla^2\vec{B}(\vec{r},t) - \frac{1}{c^2}\frac{\partial^2\vec{B}(\vec{r},t)}{\partial t^2} = -\mu_0\vec{\nabla}\times\vec{J}(\vec{r},t), \tag{5}$$

$$\nabla^2\vec{E}(\vec{r},t) - \frac{1}{c^2}\frac{\partial^2\vec{E}(\vec{r},t)}{\partial t^2} = \mu_0\frac{\partial\vec{J}(\vec{r},t)}{\partial t} + \frac{\vec{\nabla}\rho(\vec{r},t)}{\epsilon_0}\,.$$

For a beam with uniform distribution moving along z, and using $\omega = k_z v$ we get

$$\vec{J}(r,z,\omega) = \left(\frac{Q}{\pi a^2}\,e^{ik_z z}\,\hat{z} + i\frac{e^2 n_{0ec}}{m\omega}\,\vec{E}(r,z,\omega)\right), \tag{6}$$

$$\rho(r,z,\omega) = \left(\frac{Q}{\pi a^2\beta c}\,e^{ik_z z} + \frac{e^2 n_{0ec}}{m\omega^2}\,\vec{\nabla}\cdot\vec{E}(r,z,\omega)\right),$$

with $E_z(r,z,\omega)$ having the same z dependence such that $E_z(r,z,\omega) = E_z(r,\omega)\;e^{ik_z z}$. as well as $\rho(r,z,\omega)$ and $J_z(r,z,\omega)$. Due to the axial symmetry, the only non-vanishing field components excited by the beam are $E_z(r,\omega)$, $E_r(r,\omega)$ and $B_\theta(r,\omega)$. Fourier transforming eq. (5) and by accounting for TM modes only we get,

$$\left(\nabla_\perp^2 - k_z^2\right)\vec{E}(r,z,\omega) + \frac{\omega^2}{c^2}\,\vec{E}(r,z,\omega) =$$

$$\frac{ik_z Q\,e^{ik_z z}}{\epsilon_0\pi a^2\beta c\gamma_0^2}\,\hat{z} - i\omega\mu_0\vec{j}_{\rm e} + \frac{\omega_{\rm ec}^2}{\omega^2}\,\vec{\nabla}\left[\vec{\nabla}\cdot\vec{E}(r,z,\omega)\right], \tag{7}$$

where $\nabla_\perp^2$ is the transverse Laplacian operator, and γ is the relativistic factor defined as $\gamma_0^{-2} = 1-\beta^2$. By making use of the Maxwell's curl equations, the relations between the longitudinal electric field component $E_z(r,z,\omega)$ and the transverse components $E_r(r,z,\omega)$ and $B_\theta(r,z,\omega)$ are as follows,

$$E_r(r,\omega) = \frac{-i}{k_z\left(1-\beta^2\varepsilon_{\rm ec}\right)}\,\frac{{\rm d}E_z}{{\rm d}r}\,, \tag{8}$$

$$B_\theta(r,\omega) = -\frac{i\omega\mu_0\epsilon_0\epsilon_{\rm ec}}{k_z^2\left(1-\beta^2\varepsilon_{\rm ec}\right)}\,\frac{dE_z}{{\rm d}r}\,,$$

where the longitudinal dielectric function

$$\varepsilon_{\rm ec} = 1 - \frac{\omega_{\rm ec}^2}{\omega^2} \tag{9}$$

has been introduced. the z-component of $\vec{\nabla}[\vec{\nabla}\cdot\vec{E}(r,z,\omega)]$ on the right hand side of eq. (7) is rewritten in cylindrical coordinates as

$$\frac{\partial}{\partial z}\left[\vec{\nabla}\cdot\vec{E}(r,z,\omega)\right] = \left[\frac{1}{1-\beta^2\varepsilon_{\rm ec}}\frac{\partial^2}{\partial r^2} - k_z^2\right]\,E_z(r,\omega)\,e^{ik_z z}.$$

Also, using $\omega = k_z\beta c$ eqs. (7) for the excited electric field component E_z become,

$$\left(1 - \frac{\omega_{\rm ec}^2}{\omega^2}\,\frac{1}{1-\beta^2\varepsilon_{\rm ec}}\right)\frac{{\rm d}^2E_z(r,\omega)}{{\rm d}r^2} + \frac{1}{r}\frac{{\rm d}E_z(r,\omega)}{{\rm d}r} - \frac{k_z^2\varepsilon_{\rm ec}}{\gamma_0^2}\,E_z(r,\omega) = \frac{ik_z Q\Theta(a-r)}{\epsilon_0\pi a^2\beta c\gamma_0^2}, \tag{10}$$

where Θ stands for Heaviside unit step function. Within the conducting wall of coductivity S, we have the following equation for E_z,

$$\left[\frac{{\rm d}^2}{{\rm d}r^2} + \frac{1}{r}\frac{\rm d}{{\rm d}r} - \frac{k_z^2}{\underline{\gamma}^2}\right]\,E_z(r,\omega) = 0\,,\quad b\le r<\infty, \tag{11}$$

where the modified relativistic factor due to the conductivity reads

$$\underline{\gamma} = \frac{\gamma_0}{\sqrt{1 - i\mu_0\omega S\gamma_0^2/k_z^2}}\,. \tag{12}$$

SOLUTION OF THE DIFFERENTIAL EQUATION

To solve the homogeneous part of eq. (10), we follow ref. [10]. Introducing the following parameters,

$$\alpha = \frac{\omega_{\rm ec}^2}{\omega^2}\,\frac{1}{1-\beta^2\varepsilon_{\rm ec}},$$

$$\nu = \frac{\alpha/2}{1-\alpha},$$

$$\sigma_{\rm ec}^2 = \frac{k_z^2}{\gamma_0^2}\,\frac{\varepsilon_{\rm ec}}{1-\alpha} = \frac{k_z^2}{\gamma_0^2}\,\varepsilon_{\rm ec}(2\nu+1)\,,$$

and assuming a solution of the form $E_z = r^{-\nu}\,V(r)$, the homogeneous part of eq. (10) reduces to the differential equation of the modified cylindrical Bessel equation for $V(r)$, namely,

$$r^2V''(r) + \left(r - \sigma_{\rm ec}^2 r^2 - \nu^2\right)\,V(r) = 0\,. \tag{13}$$

Accordingly, the overall regular general solutions are expressed in terms of first kind I_ν and second kind K_ν modified cylindrical Bessel functions as follows,

$$E_z(r,\omega) = \begin{cases} A_1\, r^{-\nu}\, I_\nu(\sigma_{\rm ec} r) - i\dfrac{Q}{\pi a^2 \epsilon_0 \varepsilon_{\rm ec} k_z \beta c} & 0 \le r \le a \\ A_2\, r^{-\nu}\, I_\nu(\sigma_{\rm ec} r) + A_3\, r^{-\nu}\, K_\nu(\sigma_{\rm ec} r) & a \le r \le b \\ A_4\, K_0(\underline{\sigma} r) & b \le r < \infty \end{cases}$$

whith $\underline{\sigma} = k_z/\underline{\gamma}$.

The electromagnetic field components $E_r^{(\rm p,co)}$ and $B_\theta^{(\rm p,co)}$ in plasma and conducting wall regions are to be obtained from the corresponding $E_z^{(\rm p,co)}$ as follows,

$$E_r^{(\rm p)}(r,\omega) = \frac{1}{ik_z\,(1-\beta^2\epsilon_{\rm ec})}\,\frac{{\rm d}E_z^{(\rm p)}}{{\rm d}r}\ ,$$
$$B_\theta^{(\rm p)}(r,\omega) = \frac{\omega\mu_0\epsilon_0\epsilon_{\rm ec}}{ik_z^2\,(1-\beta^2\varepsilon_{\rm ec})}\,\frac{{\rm d}E_z^{(\rm p)}}{{\rm d}r}\ , \qquad (14)$$

$$E_r^{(\rm co)}(r,\omega) = \frac{\underline{\gamma}^2}{ik_z}\,\frac{{\rm d}E_z^{(\rm co)}}{{\rm d}r}\ ,$$
$$B_\theta^{(\rm co)}(r,\omega) = \frac{\omega\mu_0\epsilon_0\underline{\gamma}^2}{ik_z^2}\,\frac{{\rm d}E_z^{(\rm co)}}{{\rm d}r}\ . \qquad (15)$$

Accordingly, the field component E_r becomes as follows,

$$E_r(r,\omega) = \begin{cases} \dfrac{\sigma_{\rm ec}\, r^{-\nu}}{ik_z(1-\beta^2\varepsilon_{\rm ec})}\, A_1\, I_{\nu+1}(\sigma_{\rm ec} r) & r \le a\ , \\ \dfrac{\sigma_{\rm ec}\, r^{-\nu}}{ik_z(1-\beta^2\varepsilon_{\rm ec})}\times & \\ [A_2\, I_{\nu+1}(\sigma_{\rm ec} r) - A_3\, K_{\nu+1}(\sigma_{\rm ec} r)] & a \le r \le b \\ i\underline{\gamma}\, A_4\, K_1(\underline{\sigma} r). & b \le r < \infty \end{cases}$$

The integration constants are determined from the boundary conditions at $r = a$ and $r = b$, namely, the continuity of E_z and B_θ at $r = a$ and at $r = b$. Upon applying these boundary conditions, we obtain the following integration constants,

$$A_1 = -\left[\frac{K_{\nu+1}(\sigma_{\rm ec} a)}{I_{\nu+1}(\sigma_{\rm ec} a)} + \frac{K_\nu(\sigma_{\rm ec} b) - \eta_{\rm ec}\, K_{\nu+1}(\sigma_{\rm ec} b)}{I_\nu(\sigma_{\rm ec} b) + \eta_{\rm ec}\, I_{\nu+1}(\sigma_{\rm ec} b)}\right] A_3,$$
$$A_3 = \frac{Q a^\nu \sigma_{\rm ec} a}{i\pi a^2 \epsilon_0 \varepsilon_{\rm ec} k_z \beta c}\, I_{\nu+1}(\sigma_{\rm ec} a),$$
$$\eta_{\rm ec} = \frac{K_0(\underline{\sigma} b)}{K_1(\underline{\sigma} b)}\,\frac{\omega\epsilon_0\varepsilon_{\rm ec}}{i\underline{\gamma}(S - i\omega\epsilon_0)}\,\frac{\sigma_{\rm ec}}{k_z(1-\beta_0^2\varepsilon_{\rm ec})},$$
$$\eta = \frac{\omega\epsilon_0\gamma_0}{i\underline{\gamma}\,(S - i\omega\epsilon_0)}.$$

COUPLING IMPEDANCE

The current densities are defined in equation (6),

$$j_{z,b}(r,\omega) = \frac{Q}{\pi a^2}\ ,$$
$$j_{z,e}(r,\omega) = \frac{i\epsilon_0\,\omega_{\rm ec}^2}{\omega}\, E_z(r,\omega)\ ,$$
$$j_{r,e}(r,\omega) = \frac{i\epsilon_0\,\omega_{\rm ec}^2}{\omega}\, E_r(r,\omega). \qquad (16)$$

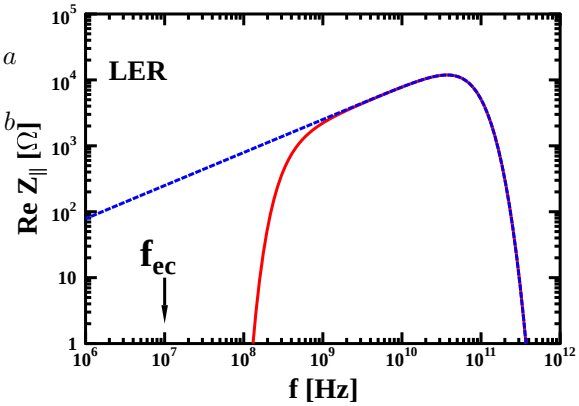

Figure 1: Dependence of the real part of the longitudinal resistive wall impedance on the excitation frequency for $f_{\rm ec} = 10$ MHz. (KEKB LER). The blue dotted line shows the impedance without electron cloud and the full red line with EC.

The longitudinal coupling impedance for the beam monopole source term is obtained as follows,

$$Z_\parallel(\omega) = -\frac{1}{Q^2}\int_\Omega E_z(\vec{r},\omega)\cdot j_b^*(\vec{r},\omega)\,{\rm d}^3 r$$
$$= -\frac{2L}{Qa^2}\int_0^a \left[A_1\frac{I_\nu(\sigma_1 r)}{r^\nu} - i\frac{Q}{\pi a^2\epsilon_0\varepsilon_{\rm ec}k_z\beta c}\right] r{\rm d}r, \quad (17)$$

where L is the circumference of the ring. This integral can be solved to yield the closed form expression

$$Z_\parallel(\omega) = -\frac{2L}{Qa^2}\left[A_1\left(\frac{I_{\nu-1}(\sigma_{\rm ec} a)}{\sigma_{\rm ec} a^{\nu-1}} - \frac{\sigma_{\rm ec}^{\nu-2}}{2^{\nu-1}\Gamma(\nu)}\right) - i\frac{Q}{\pi a^2\epsilon_0\varepsilon_{\rm ec}k_z\beta c}\,\frac{a^2}{2}\right]. \qquad (18)$$

For $\omega_{\rm ec} = 0$, the impedance above reduces into the known form [10]

$$Z_\parallel(\omega) = i\,\frac{nZ_0}{2\beta\gamma^2}\,\frac{4\gamma_0^2}{k_z^2 a^2}\left[1 - 2I_1^2(\sigma_0 a)F\right] \qquad (19)$$

with the constant

$$F = \frac{K_1(\sigma_0 a)}{I_1(\sigma_0 a)} + \frac{K_0(\sigma_0 b) - \eta\dfrac{K_0(\underline{\sigma} b)}{K_1(\underline{\sigma} b)}K_1(\sigma_0 b)}{I_0(\sigma_0 b) + \eta\dfrac{K_0(\underline{\sigma} b)}{K_1(\underline{\sigma} b)}I_1(\sigma_0 b)}.$$

NUMERICAL EXAMPLES AND DISCUSSION

The longitudinal coupling impedances above are calculated for various circular machines with idealized machine parameters and different strengths of the electron cloud density. In Fig. 1 at the example of the KEKB LER with the assumed electron plasma frequency of 10 MHz is shown the real part of the coupling impedance with (full red

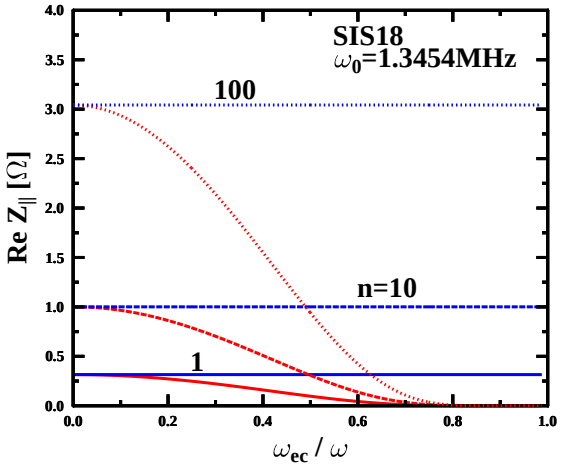

Figure 2: Dependence of the real part of the longitudinal resistive wall impedance on the ratio of electron cloud plasma frequency to excitation frequency $\omega = n\omega_0$ (GSI–SIS18). The blue lines show the impedance for $\omega_{ec} = 0$ and n indicates the harmonic number.

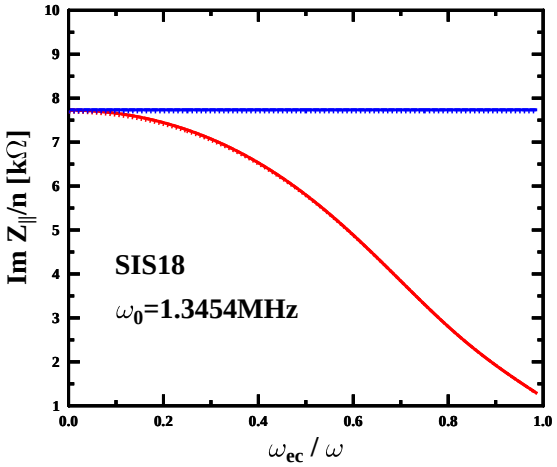

Figure 4: Comparison between the imaginary parts of the longitudinal resistive wall impedance per harmonic (GSI–SIS18) with and without electron cloud. Same notation as in Fig. 2.

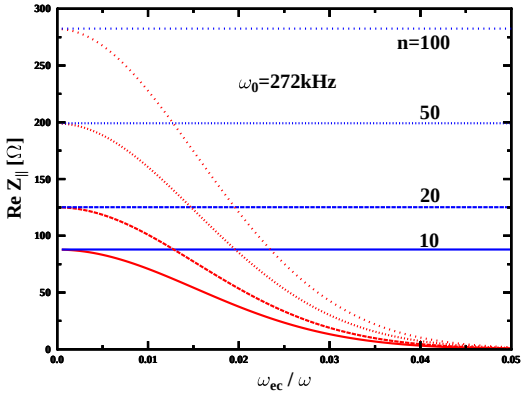

Figure 3: Same as Fig. 2 but for the CERN SPS. Note the change of scale of the abscissa.

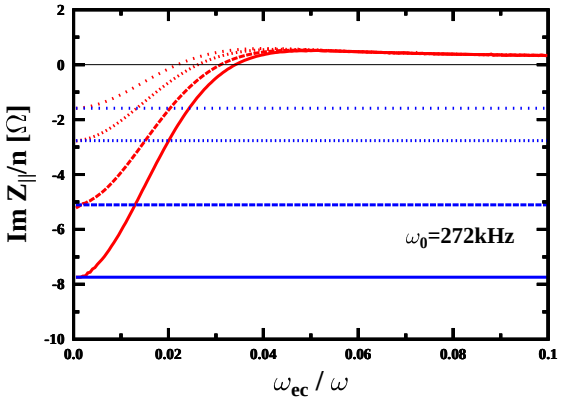

Figure 5: Imaginary part of the longitudinal resistive wall impedance per harmonic (CERN SPS).

line) and without (blue dotted line) presence of the electron cloud. The coupling impedance is depleted for all excitation frequencies up to about 500 MHz, i.e. almost two orders of magnitude above the EC plasma frequency. Similarly, in Fig. 2 for SIS18 and Fig. 3 for SPS is shown the dependence of the real part of the longitudinal coupling impedance on the electron cloud plasma frequency ω_{ec} (or $f = \omega_{ec}/2\pi$) for various excitation frequencies $f = nf_0$, where n is the harmonic number and f_0 is the revolution frequency. Due to the dependence of the dielectric function in eq. (9) on ω_{ec}/ω (or f_{ec}/f) this ratio is chosen. They exhibit a decrease of the real part of the resistive–wall impedance with increasing EC density due to the plasma shielding of the wall, and therefore a reduction in the current induced by the beam in the wall of beam–pipe. Equivalently, the coupling impedance increases with increasing excitation frequency.

Analogously, in Fig. 4 for SIS18 and Fig. 5 for SPS are shown the imaginary parts. In contrast to the real part, the total imaginary part consists of two parts, the resitive wall and the space charge $Z_{||}(\omega_{ec} = 0, S = \infty)$ contributions. Here the total imaginary part of the coupling impedance for SIS18 (space charge + resistive–wall) is positive according to our physical conventions (negative imaginary in engineering conventions), and therefore the EC as a whole acts as a capacitive medium for all frequencies such that $\omega > \omega_{ec}$. Its resistive wall part, however, is negative, thus inductive.

For excitation frequencies below the plasma frequency the EC will act as an inductive medium with negative imaginary part. For the SPS, on the other hand, the imaginary part is negative and turns capacitive only in the presence of strong electron fields.

Using a simple analogy, we can explain the above properties of the impedance in the presence of the EC. The total current in the electron cloud region is composed of dis-

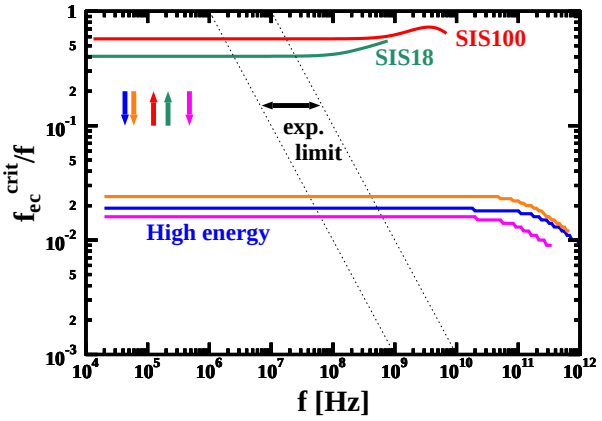

Figure 6: Fraction of critical electron cloud frequency where the longitudinal resistive wall impedance is half depleted as compared to the excitation frequency. The dahed lines idicates the measured value of electron cloud density of 10^{12} m^{-3} and 10^{11} m^{-3} in the SPS and LER. The arrows point to the respective revolution frequencies.

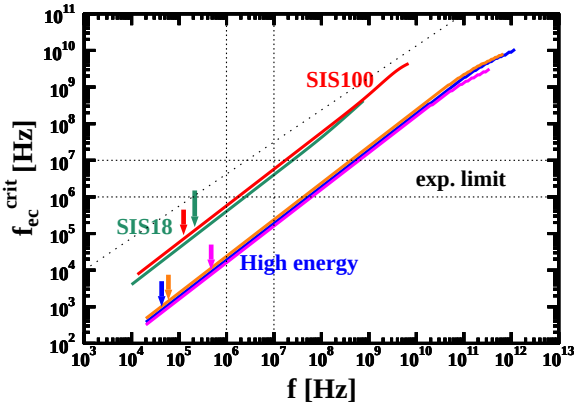

Figure 7: Same as Fig. 6 but critical electron cloud frequency vs. frequency

placement and EC currents (plasma), respectively,

$$\vec{J}(\vec{k},\omega) = -i\,\omega\,C_{\rm ec}\,\vec{E} - \frac{1}{i\omega\,L_{\rm ec}}\,\vec{E}.$$

Here $C_{\rm ec} = \epsilon_0$ ist the capacitance per unit length and $L_{\rm ec} = m_{\rm e}/n_{\rm ec}e^2$ is the inductance times unit length. We introduce the Plasma (Electric) Impedivity $\hat{z}_{\rm e}$ as follows,

$$\vec{E} = \hat{z}_{\rm e}\,\vec{J},\;\; \hat{z}_{\rm e} = -\frac{i\omega\,L_{\rm ec}}{1-\omega^2\,C_{\rm ec}L_{\rm ec}},$$
$$\omega_{\rm ec} = \frac{1}{\sqrt{L_{\rm ec}C_{\rm ec}}} = \sqrt{n_{\rm ec}e^2/m\epsilon_0}.$$

As can be seen from the expression for $\hat{z}_{\rm e}$, the EC act as a capacitive plasma for $\omega > \omega_{\rm ec}$, and as inductive plasma for $\omega < \omega_{\rm ec}$. By ignoring Joule heating of the electron cloud (energy loss due to collisions), there will be a total cancellation between displacement and plasma currents at mode frequencies such that $\omega = \omega_{\rm ec}$, namely, $\vec{J}(\vec{r},\omega) = \vec{J}_D + \vec{J}_{\rm ec} = 0$.

There is a striking difference between the results for the low energy machines SIS18, SIS100 and the high energy machines SPS, PS, and LER. namely that the latter deplete their impedance for EC plasma frequencies already of the order of 2% of the excitation frequency whereas this ratio is about 50% for the SIS18. This behaviour is studied systematically for all machines under consideration and the critical ratios $\omega_{\rm ec}^{\rm crit}/\omega = f_{\rm ec}^{\rm crit}/f$ are extracted where $\omega_{\rm ec}/\omega$ fall of to 50% from their original values. These ratios are shown in Fig. 6. Experimental EC densities measured in SPS and LER are in the range $n_{\rm ec} = 10^{11}\cdots10^{12}$ m^{-3}, indicated by the dotted lines in Figs. 6, 7. This means that instabilities in the low energy machines are expected for frequencies below $2\cdots20$ MHz whereas in the high energy machines instabilities are expected in a much wider frequency range below $50\cdots500$ MHz. Fig. 7 shows the same as Fig. 6 but as the critical electron cloud density vs. excitation frequency.

SURFACE-WAVE-SUSTAINED MODES

Electromagnetic waves cannot propagate in an over-dense plasma if the plasma frequency is larger than the excitation frequency, $\omega_{\rm ec} > \omega$, i.e. when the beam is completely shielded by the electromagnetic field of the electron cloud. Then the waves are reflected at the conducting surface due to the skin effect and become evanescent waves. Their penetration depth corresponds roughly to the skin depth $\delta_s \approx c(\omega_{\rm ec}^2 - \omega^2)^{-1/2}$. This may give rise to heating a plasma rather than damping it. The waves then do not travel any more in the radial direction but rather propagate along the plasma surface. The wave energy is then transferred to the plasma by the evanescent wave which enters the plasma perpendicular to its surface and decays exponentially with the skin depth. Due to the heating process, the real part of the impedance becomes negative. This transfer mechanism allows to support over-dense plasmas with electron plasma frequencies beyond the excitation frequency. For even higher excitation frequencies, $\omega_{\rm ec}/\omega > \sqrt{2}$, these waves do not propagate any more along the surface bur are rather overdamped in the longitudinal direction. Such overdamped surface waves have been studied e.g. in ref. [11].

Our analysis for a relatively weak beam ($\gamma = 1.0122$) in SIS18 shown in Figs. 8,9 indicates that one can distinguish three regions of a beam embedded in an overdamped plasmas: (i) No waves exist for $1 < \omega_{\rm ec}/\omega \lesssim 1.05$; (ii) In the intermediate region of evanescent waves, $1.05 \lesssim \omega_{\rm ec}/\omega \lesssim \sqrt{2}$ the real part of the impedance is negative and the imaginary part is positive, thus capacitive due to the strong magnetic field; (iii) Overdamped surface waves $\omega_{\rm ec}/\omega > \sqrt{2}$ with positive real part and negative imaginary part exist for $\omega_{\rm ec}/\omega > \sqrt{2}$ in analogy to the case of $\omega > \omega_{\rm ec}^{\rm crit}$ of the previous chapter The latter two regions are separated by a resonance transition. Due to the presence of the weak beam the critical value $\sqrt{2}$ is only shifted slightly. An case of more intense beams it is shifted substantially to higher values.

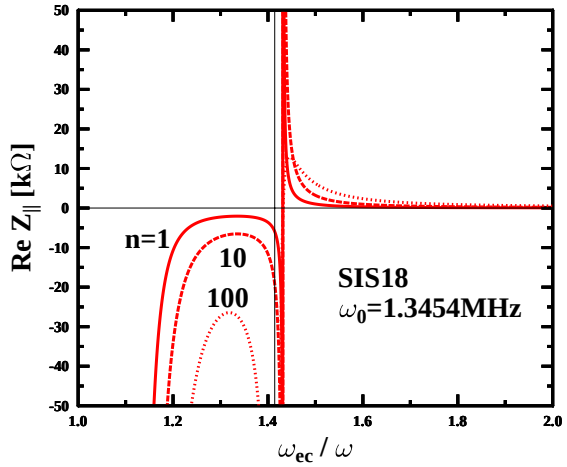

Figure 8: Same as Fig. 2 but for $\omega_{\rm ec} > \omega$. The thin vertical line points to the ower limit of surface waves $\omega_{\rm ec}/\omega = \sqrt{2}$ (SIS18).

SUMMARY AND OUTLOOK

The effect of shielding of a beam by a homogeneous electron cloud on the coupling impedance has been calculated as a function of the electon cloud density. It has been found that the depletion of the coupling impedance is complete not as expected at the excitation frequency corresponding to the plasma frequency of the EC but, for high energy circular machines, already for much lower electron cloud densities.

The theory does not yet account for resonance effects at the singularity at $\omega = \omega_{\rm ec}$. The calculations, hence, must be extended to include Joule heating by losses from the imaginary part of ω and to small excitation frequencies $\omega < \omega_{\rm ec}$.

The same theory can also serve for the calculation of modifications of the electric field of the beam due to the presence of an electron cooler. The electron beams of present electron coolers generate amperes of current and, hence, shield the beam substantially.

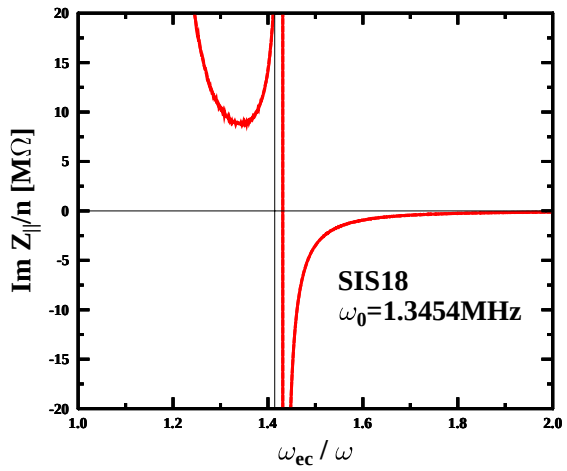

Figure 9: Same as Fig. 4 but for $\omega_{\rm ec} > \omega$ (SIS18).

ACKNOWLEDGMENTS

One of us (A.A.) thanks the Fair Accelerator Theory Group of GSI Darmstadt for frequent invitations. He also likes to thank the Council of Scientific Research of Yarmouk University, Irbid, Jordan, for supporting this work by the grant 8/2007. He also likes to thank the Arab Fund for Economic and Social Development (AFESD, State of Kuwait) for the financial support of his stay at GSI-Darmstadt (Germany) via their Fellowship Award. We also acknowledge the support of the European Community *Research Infrastructures Action* under the FP6 programme: Structuring the European Research Area - Specific Support Action - Design Study (contract 515873 - DIRAC-secondary-Beams).

REFERENCES

[1] F. Zimmermann, *Electron-Cloud Studies for the Low Energy Ring of KEKB*, CERN-SL-Note-2000-004 AP.

[2] M. Giovannozzi, Métral, G. Rumolo, and F. Zimmermann, Phys. Rev. ST Accel. Beams **6** (2003) 010101.

[3] G. Rumolo, A. Z. Ghalam, T. Katsouleas, C. K. Huang, V. K. Decyk, C. Ren, W. B. Mori F. Zimmermann, and F. Ruggiero, Phys. Rev. ST Accel. Beams **6** (2003) 081002.

[4] W. Fischer, J.M. Brennan, M. Blaskiewicz, and T. Satogata, Proc. ECLOUD'02 Workshop, CERN, 15-18 April 2002, CERN Yellow Report CERN-2002-001.

[5] F. Zimmermann, Phys. Rev. ST Accel. Beams **7** (2004) 124801.

[6] *http://ab-abp-rlc.web.cern.ch/ab-abp-rlc-ecloud.*

[7] G. Rumolo and F. Zimmermann, Phys. Rev. ST Accel. Beams **5** (2002) 121002.

[8] G. Rumolo and Métral, Proc. 9th Int. Computational Accelerator Physics Conference, Oct. 2-6, 2006, Chamonix Mont-Blanc, France, ICAP06, *http://accelconf.web.cern.ch, MOA2IS02.*

[9] P. Mulser, *High Power Laser-Matter Interaction*, Springer, Berlin 2006

[10] A.M. Al - Khateeb, O. Boine-Frankenheim, R.W. Hasse, and I. Hofmann, Phys. Rev. E **71**, 026501-1 (2005).

[11] A. Boardman, *Electromagnetic Surface Waves*, Wiley, N.Y. 1982.